Dynamic Analysis

2D Ball Balancer Project

Prepared by:

Ege Özbülbül

June 2025

Progress Notes

- ✓ Added Appendix for Parameter Identification (Appendix B)
- ✓ Ignored 2 RHS terms for the simplified EOM
- ☐ Add the MATLAB code for the numerical solution for the full EOM
- ☐ Add SIMULINK images and solutions for the full and simplified EOM
- ☐ Add schematics for the Kinematic Relationships and Energy Expressions
- ☐ Euler-Lagrange RHS terms need refinement
- ☐ Determine geometric parameters and calculate EOMs again by using those
- ☐ Complete Simulation Validation and Validation Envelope
- ☐ Fix documentation arrangement

Contents

1 Introduction

This document presents the dynamic modeling and analysis of the 2D Ball Balancer system. The report covers a detailed description of the system, definitions of all notations, the derivation of kinematic relationships, energy expressions, and the complete formulation using the Euler-Lagrange method. The goal is to establish a mathematical model that serves as a foundation for simulation, control, and further development of the system.

The document is structured as follows:

- **Section 2: System Description** — outlines the mechanical setup and main components
- **Section 3: Nomenclature** — lists all variables and parameters with definitions
- **Section 4: Kinematic Relationships** — derives position, velocity, and acceleration expressions
- **Section 5: Energy Expressions** — formulates kinetic and potential energy terms
- **Section 6: Lagrangian Formulation** — constructs the system's Lagrangian
- **Section 7: Euler-Lagrange Equations** — derives the equations of motion
- **Section 8: Model Simplifications and Assumptions** — simplifies the equations of motion and lists the assumptions
- **Appendix** — shows the related codes, schematics, tables, graphs

All variables are given in SI units unless otherwise stated.

2 System Description

The 2D Ball Balancer is a electromechanical system designed to control the position of a spherical ball on a rigid, square platform by tilting the platform along two orthogonal axes (X and Y). The system consists of the following primary components:

- **Platform:** A flat, square plate on which the ball can move freely. The platform is supported in a way that allows independent rotation about the X and Y axes.
- **Ball:** A solid, uniform sphere that rolls passively on the surface of the platform under the influence of gravity and platform inclination.
- **Actuation Mechanism:** Each axis is actuated by a servo motor connected to a rack and pinion mechanism, providing precise adjustment of the platform's tilt angle in each direction.

The physical modeling considers the effects of gravity and relevant frictional forces acting on the ball.

3 Nomenclature

- x : Position of the ball along the X-axis (mm)
- y : Position of the ball along the Y-axis (mm)
- θ_x : Tilt angle of the platform with respect to the horizontal, X-axis (radian)
- θ_y : Tilt angle of the platform with respect to the horizontal, Y-axis (radian)
- ψ_x : Rotation angle of the ball about the X-axis (radian)
- ψ_y : Rotation angle of the ball about the Y-axis (radian)
- ϕ_x : Rotation angle of the X-axis servo motor (radian)
- ϕ_y : Rotation angle of the Y-axis servo motor (radian)
- ΔL_x : Distance travelled by the X-axis rack as the servo rotates (mm)
- ΔL_y : Distance travelled by the Y-axis rack as the servo rotates (mm)
- r_p : Pinion radius (mm)
- r_{ball} : Radius of the ball (m)
- OS : Offset distance where the racks are attached from the X and Y axes
- L : Platform length (mm)
- g : Gravitational acceleration (9.81 m/s^2)
- m_{ball} : Mass of the ball (kg)
- m_{platform} : Mass of the platform (kg)
- m_{rack} : Mass of the rack (kg)
- m_{pinion} : Mass of the pinion (kg)
- I_{ball} : Moment of inertia of the ball (kg·m^2)
- I_{platform} : Moment of inertia of the platform (kg·m^2)
- I_{rack} : Moment of inertia of the rack (kg·m^2)
- I_{pinion} : Moment of inertia of the pinion (kg·m^2)

4 Kinematic Relationships

$$\Delta L_x = r_p\,\phi_x, \qquad \Delta L_y = r_p\,\phi_y \tag{1}$$

$$d = L - OS \tag{2}$$

$$\theta_x = \arctan\left(\frac{\Delta L_x}{d}\right), \qquad \theta_y = \arctan\left(\frac{\Delta L_y}{d}\right) \tag{3}$$

$$\phi_x = \frac{d}{r_p}\tan\theta_x, \qquad \phi_y = \frac{d}{r_p}\tan\theta_y \tag{4}$$

$$\dot{\psi}_x = \frac{\dot{x}}{r_{\text{ball}}}, \qquad \dot{\psi}_y = \frac{\dot{y}}{r_{\text{ball}}} \tag{5}$$

Explanation of Equations:

(1) Defines the linear displacement of the rack as a function of the servo rotation angle.

(2) Describes the effective lever arm between the servo axis and the platform pivot point.

(3) Relates the platform tilt angles to the rack displacements via inverse tangent geometry.

(4) Expresses the servo angles as functions of the platform tilt angles.

(5) Maps the translational velocities of the ball to rotational velocities in each axis.

5 Energy Expressions

In this section, the energy expressions of the system are presented for both the decoupled and coupled cases. First, all energies are derived under the assumption that the system is decoupled (each axis operates independently). Subsequently, the corresponding coupled expressions are provided for a more general and physically accurate model.

This section assumes that the energy formulas are only dependent on the rotation of one motor per each axis

5.1 Kinetic Energy

Kinetic Energy of the system is composed of both Translational and Rotational energies

5.1.1 Translational Kinetic Energy

The total translational kinetic energy is the sum of the kinetic energies of the ball and the racks, each moving along the X and Y axes.

- **Ball (X-axis):**

$$KE_{\text{trans, ball, } x} = \frac{1}{2} m_{\text{ball}} \, \dot{x}^2$$

- **Ball (Y-axis):**

$$KE_{\text{trans, ball, } y} = \frac{1}{2} m_{\text{ball}} \, \dot{y}^2$$

- **Rack (X-axis):**

$$KE_{\text{trans, rack, } x} = \frac{1}{2} m_{\text{rack}} \, (\dot{\Delta L}_x)^2 = \frac{1}{2} m_{\text{rack}} \, (r_p \, \dot{\phi}_x)^2$$

- **Rack (Y-axis):**

$$KE_{\text{trans, rack, } y} = \frac{1}{2} m_{\text{rack}} \, (\dot{\Delta L}_y)^2 = \frac{1}{2} m_{\text{rack}} \, (r_p \, \dot{\phi}_y)^2$$

5.1.2 Rotational Kinetic Energy

The total rotational kinetic energy consists of the ball, platform, and pinion for both X and Y axes.

- **Ball (X-axis):**

$$I_{\text{ball}} = \frac{2}{5} m_{\text{ball}} \, r_{\text{ball}}^2$$

The ball is modeled as a solid sphere. Its rotational velocity about the X-axis is $\dot{\psi}_x = \frac{\dot{x}}{r_{\text{ball}}}$. Therefore,

$$KE_{\text{rot, ball, } x} = \frac{1}{2} I_{\text{ball}} \, \dot{\psi}_x^2 = \frac{1}{2} \cdot \frac{2}{5} m_{\text{ball}} \, r_{\text{ball}}^2 \left(\frac{\dot{x}}{r_{\text{ball}}} \right)^2$$

- **Ball (Y-axis):**

$$KE_{\text{rot, ball, } y} = \frac{1}{2} I_{\text{ball}} \, \dot{\psi}_y^2 = \frac{1}{2} \cdot \frac{2}{5} m_{\text{ball}} \, r_{\text{ball}}^2 \left(\frac{\dot{y}}{r_{\text{ball}}} \right)^2$$

- **Platform (X-axis):**

$$I_{\text{platform}} = \frac{1}{12} m_{\text{platform}} L^2 + m_{\text{platform}} \left(\frac{L}{2} - OS \right)^2$$

  The moment of inertia is calculated using the parallel axis theorem (Steiner's theorem), since the axis of rotation is offset from the platform's center. The rotational velocity is $\dot{\theta}_x$. Therefore,

$$KE_{\text{rot, platform, } x} = \frac{1}{2} I_{\text{platform}} \, \dot{\theta}_x^2$$

- **Platform (Y-axis):**

$$KE_{\text{rot, platform, } y} = \frac{1}{2} I_{\text{platform}} \, \dot{\theta}_y^2$$

- **Pinion (X-axis):**

$$I_{\text{pinion}} = \frac{1}{2} m_{\text{pinion}} r_p^2$$

  The pinion is assumed as a solid cylinder. Its rotational velocity is $\dot{\phi}_x$. Therefore,

$$KE_{\text{rot, pinion, } x} = \frac{1}{2} I_{\text{pinion}} \, \dot{\phi}_x^2 = \frac{1}{2} \cdot \frac{1}{2} m_{\text{pinion}} r_p^2 \dot{\phi}_x^2$$

- **Pinion (Y-axis):**

$$KE_{\text{rot, pinion, } y} = \frac{1}{2} I_{\text{pinion}} \, \dot{\phi}_y^2 = \frac{1}{2} \cdot \frac{1}{2} m_{\text{pinion}} r_p^2 \dot{\phi}_y^2$$

5.2 Potential Energy

The total potential energy is the sum of the gravitational potential energies of the ball, platform, and rack for both the X and Y axes.

- **Ball (X-axis):**
  - $h_{1,x} = \dfrac{r_{\text{ball}}}{\cos \theta_x}$: Vertical distance from the center of the ball to the platform (X component).
  - $h_{2,x} = (L - x - \alpha_x) \sin \theta_x$: Vertical distance from the contact point to the ground (X component), where $\alpha_x = r_{\text{ball}} \tan \theta_x$.

  - The total height of the ball's center above the ground is:
  - The ball's potential energy:

$$h_x = h_{1,x} + h_{2,x} = \frac{r_{\text{ball}}}{\cos\theta_x} + (L - x - r_{\text{ball}} \tan\theta_x) \sin\theta_x$$
$$V_{\text{ball},\,x} = m_{\text{ball}}\, g\, h_x$$

- **Ball (Y-axis):**
  - $h_{1,y} = \dfrac{r_{\text{ball}}}{\cos\theta_y}$
  - $h_{2,y} = (L - y - \alpha_y)\sin\theta_y$, where $\alpha_y = r_{\text{ball}} \tan\theta_y$
  - $h_y = h_{1,y} + h_{2,y}$
  - The ball's potential energy:

$$V_{\text{ball},\,y} = m_{\text{ball}}\, g\, h_y$$

- **Platform (X-axis):**
  - The center of mass is at $h_{\text{platform},\,x} = \frac{L}{2}\sin\theta_x$ above the ground.
  - The platform's potential energy:

$$V_{\text{platform},\,x} = m_{\text{platform}}\, g\, h_{\text{platform},\,x}$$

- **Platform (Y-axis):**
  - $h_{\text{platform},\,y} = \frac{L}{2}\sin\theta_y$
  - The platform's potential energy:

$$V_{\text{platform},\,y} = m_{\text{platform}}\, g\, h_{\text{platform},\,y}$$

- **Rack (X-axis):**
  - The rack's vertical position is $h_{\text{rack},\,x} = \Delta L_x = r_p\, \phi_x$
  - The rack's potential energy:

$$V_{\text{rack},\,x} = m_{\text{rack}}\, g\, h_{\text{rack},\,x} = m_{\text{rack}}\, g\, r_p\, \phi_x$$

- **Rack (Y-axis):**
  - $h_{\text{rack},\,y} = \Delta L_y = r_p\, \phi_y$
  - The rack's potential energy:

$$V_{\text{rack},\,y} = m_{\text{rack}}\, g\, r_p\, \phi_y$$

5.3 Total Energy Expressions

Below, the **total kinetic energy** for each axis is given. All terms are shown in their most *expanded* form.

Total Kinetic Energy for the X-axis (most expanded form):

$$
\begin{aligned}
T_x \;=\; & \underbrace{\frac{1}{2} m_{\text{ball}} \dot{x}^2}_{\text{Ball translation}} + \underbrace{\frac{1}{2}\left(\frac{2}{5} m_{\text{ball}} r_{\text{ball}}^2\right)\left(\frac{\dot{x}}{r_{\text{ball}}}\right)^2}_{\text{Ball rotation}} \\
& + \underbrace{\frac{1}{2} m_{\text{rack}} (r_p \dot{\phi}_x)^2}_{\text{Rack translation}} + \underbrace{\frac{1}{2}\left(\frac{1}{2} m_{\text{pinion}} r_p^2\right) \dot{\phi}_x^2}_{\text{Pinion rotation}} \\
& + \underbrace{\frac{1}{2}\left[\frac{1}{12} m_{\text{platform}} L^2 + m_{\text{platform}} \left(\frac{L}{2} - OS\right)^2\right] \dot{\theta}_x^2}_{\text{Platform}}
\end{aligned}
$$

Compact form (X-axis):

$$
T_x = \frac{7}{10} m_{\text{ball}} \dot{x}^2 + \frac{1}{2} m_{\text{rack}} r_p^2 \dot{\phi}_x^2 + \frac{1}{4} m_{\text{pinion}} r_p^2 \dot{\phi}_x^2 + \frac{1}{2} m_{\text{platform}} \left[\tfrac{L^2}{12} + \left(\tfrac{L}{2} - OS\right)^2\right] \dot{\theta}_x^2
$$

(The ball terms are merged, and rack/pinion inertia terms are grouped for clarity.)

Total Kinetic Energy for the Y-axis (most expanded form):

$$
\begin{aligned}
T_y \;=\; & \underbrace{\frac{1}{2} m_{\text{ball}} \dot{y}^2}_{\text{Ball translation}} + \underbrace{\frac{1}{2}\left(\frac{2}{5} m_{\text{ball}} r_{\text{ball}}^2\right)\left(\frac{\dot{y}}{r_{\text{ball}}}\right)^2}_{\text{Ball rotation}} \\
& + \underbrace{\frac{1}{2} m_{\text{rack}} (r_p \dot{\phi}_y)^2}_{\text{Rack translation}} + \underbrace{\frac{1}{2}\left(\frac{1}{2} m_{\text{pinion}} r_p^2\right) \dot{\phi}_y^{\,2}}_{\text{Pinion rotation}} \\
& + \underbrace{\frac{1}{2}\left[\frac{1}{12} m_{\text{platform}} L^2 + m_{\text{platform}} \left(\frac{L}{2} - OS\right)^2\right] \dot{\theta}_y^2}_{\text{Platform}}
\end{aligned}
$$

(All substitutions for y-axis are completely analogous to the x-axis. Only velocity variables change: $\dot{y}$, $\dot{\phi}_y$, $\dot{\theta}_y$.)

Compact form (Y-axis):

$$
T_y = \frac{7}{10} m_{\text{ball}} \dot{y}^2 + \frac{1}{2} m_{\text{rack}} r_p^2 \dot{\phi}_y^2 + \frac{1}{4} m_{\text{pinion}} r_p^2 \dot{\phi}_y^2 + \frac{1}{2} m_{\text{platform}} \left[\tfrac{L^2}{12} + \left(\tfrac{L}{2} - OS\right)^2\right] \dot{\theta}_y^2
$$

6 Lagrangian Formulation

$$\mathcal{L} = T - V \tag{6}$$

The Lagrangian $\mathcal{L}$ is defined as the difference between the total kinetic energy T and the total potential energy V of the system.

In the total kinetic and potential energy expressions, the angles θ_x and θ_y can be eliminated in favor of the measurable pinion (servo) angles ϕ_x and ϕ_y by using the pure kinematic link:

$$\theta_{x/y} = \arctan\left(\frac{r_p\,\phi_{x/y}}{d}\right), \qquad d := L - OS$$

where r_p is the pinion radius, L is the platform length, and OS is the offset distance.

The corresponding time-derivative is:

$$\dot{\theta}_{x/y} = \frac{r_p\,d\,\dot{\phi}_{x/y}}{d^2 + r_p^2\phi_{x/y}^2}$$

This substitution allows all energy and equation-of-motion expressions to be rewritten in terms of $\phi_{x/y}$ only, i.e., the servo (input) angle.

For convenience, the following trigonometric identities will be used throughout the derivation:

$$\tan\theta_{x/y} = \frac{r_p\,\phi_{x/y}}{d}$$

$$\cos\theta_{x/y} = \frac{d}{\sqrt{d^2 + r_p^2\phi_{x/y}^2}}$$

$$\sin\theta_{x/y} = \frac{r_p\,\phi_{x/y}}{\sqrt{d^2 + r_p^2\phi_{x/y}^2}}$$

After substituting both the kinematic link ($\theta_{x/y}$) and $d = L - OS$ into all expressions, the total kinetic and potential energies are fully rewritten in terms of the servo angle $\phi_{x/y}$, which is the true system input. The resulting compact forms for each axis are as follows:

6.1 Kinetic Energy (for x/y axis):

$$T_{x/y} = \frac{7}{10}\, m_{\text{ball}}\, \dot{x/y}^{\,2} + \left(\frac{1}{2} m_{\text{rack}} + \frac{1}{4} m_{\text{pinion}}\right) r_p^2 \dot{\phi}_{x/y}^2$$

$$+ \frac{1}{2} m_{\text{platform}} \left[\frac{L^2}{12} + \left(\frac{L}{2} - OS\right)^2\right] \left(\frac{r_p (L - OS)}{(L - OS)^2 + r_p^2 \phi_{x/y}^2}\right)^2 \dot{\phi}_{x/y}^2$$

6.2 Potential Energy (for x/y axis):

$$V_{x/y} = -\, m_{\text{ball}} g\, \frac{r_{\text{ball}} \sqrt{(L - OS)^2 + r_p^2 \phi_{x/y}^2}}{L - OS}$$

$$- m_{\text{ball}} g \left(L - x/y - r_{\text{ball}} \frac{r_p \phi_{x/y}}{L - OS}\right) \frac{r_p \phi_{x/y}}{\sqrt{(L - OS)^2 + r_p^2 \phi_{x/y}^2}}$$

$$- \frac{1}{2} m_{\text{platform}} g L\, \frac{r_p \phi_{x/y}}{\sqrt{(L - OS)^2 + r_p^2 \phi_{x/y}^2}}$$

$$- m_{\text{rack}} g r_p \phi_{x/y}$$

Below, the Lagrangian is written separately for each axis (x and y), using the fully substituted forms for kinetic and potential energies.

6.3 Lagrangian for the X-axis:

$$\mathcal{L}_x = \frac{7}{10} m_{\text{ball}} \dot{x}^2 + \left(\frac{1}{2} m_{\text{rack}} + \frac{1}{4} m_{\text{pinion}} \right) r_p^2 \dot{\phi}_x^2$$

$$+ \frac{1}{2} m_{\text{platform}} \left[\frac{L^2}{12} + \left(\frac{L}{2} - OS \right)^2 \right] \left(\frac{r_p (L - OS)}{(L - OS)^2 + r_p^2 \phi_x^2} \right)^2 \dot{\phi}_x^2$$

$$- m_{\text{ball}} g \, \frac{r_{\text{ball}} \sqrt{(L - OS)^2 + r_p^2 \phi_x^2}}{L - OS}$$

$$- m_{\text{ball}} g \left(L - x - r_{\text{ball}} \frac{r_p \phi_x}{L - OS} \right) \frac{r_p \phi_x}{\sqrt{(L - OS)^2 + r_p^2 \phi_x^2}}$$

$$- \frac{1}{2} m_{\text{platform}} g L \, \frac{r_p \phi_x}{\sqrt{(L - OS)^2 + r_p^2 \phi_x^2}}$$

$$- m_{\text{rack}} g r_p \phi_x$$

6.4 Lagrangian for the Y-axis:

$$\mathcal{L}_y = \frac{7}{10} m_{\text{ball}} \dot{y}^2 + \left(\frac{1}{2} m_{\text{rack}} + \frac{1}{4} m_{\text{pinion}} \right) r_p^2 \dot{\phi}_y^2$$

$$+ \frac{1}{2} m_{\text{platform}} \left[\frac{L^2}{12} + \left(\frac{L}{2} - OS \right)^2 \right] \left(\frac{r_p (L - OS)}{(L - OS)^2 + r_p^2 \phi_y^2} \right)^2 \dot{\phi}_y^2$$

$$- m_{\text{ball}} g \, \frac{r_{\text{ball}} \sqrt{(L - OS)^2 + r_p^2 \phi_y^2}}{L - OS}$$

$$- m_{\text{ball}} g \left(L - y - r_{\text{ball}} \frac{r_p \phi_y}{L - OS} \right) \frac{r_p \phi_y}{\sqrt{(L - OS)^2 + r_p^2 \phi_y^2}}$$

$$- \frac{1}{2} m_{\text{platform}} g L \, \frac{r_p \phi_y}{\sqrt{(L - OS)^2 + r_p^2 \phi_y^2}}$$

$$- m_{\text{rack}} g r_p \phi_y$$

7 Euler-Lagrange Equations

The Euler-Lagrange equations provide the fundamental link between the Lagrangian formulation and the equations of motion (EOM) for the system. For each generalized coordinate q_i, the standard form is:

$$\frac{d}{dt}\left(\frac{\partial \mathcal{L}}{\partial \dot{q}_i}\right) - \frac{\partial \mathcal{L}}{\partial q_i} = Q_i$$

where L is the Lagrangian, q_i are the generalized coordinates (x, y, ϕ_x, ϕ_y), and Q_i represents generalized forces (including dissipative/frictional effects).

7.1 Left-Hand Side (LHS): Inertial and Conservative Terms

The left-hand side of the Euler-Lagrange equation collects all the inertial (mass-related) and conservative (energy-preserving) terms for each coordinate. This represents the system dynamics excluding non-conservative effects like friction.

The general LHS for each coordinate is:

$$\text{LHS}(q_i) = \frac{d}{dt}\left(\frac{\partial \mathcal{L}}{\partial \dot{q}_i}\right) - \frac{\partial \mathcal{L}}{\partial q_i}$$

7.1.1 LHS for x and y coordinates

The explicit left-hand side of the equations of motion for x and y are presented, derived from the substituted Lagrangians above.

LHS of x(t): Below is the explicit equation of motion for the x-axis, as derived from the Lagrangian. This form includes all inertial, gravitational, and nonlinear geometric effects, and is ready to be used for simulation or control design:

$$
\begin{aligned}
LHS_x =& \frac{7}{5} m_{\text{ball}}\, \ddot{x}(t) \\
&+ g\, m_{\text{rack}}\, r_p\, \phi_x(t) \\
&- \frac{g\, m_{\text{ball}}\, r_p\, \dot{\phi_x}(t) \left[x(t) - L + \frac{r_{\text{ball}}\, r_p\, \phi_x(t)}{L - OS} \right]}{\sqrt{r_p^2\, \phi_x(t)^2 + (L - OS)^2}} \\
&- \frac{g\, m_{\text{ball}}\, r_p\, \phi_x(t) \left[\dot{x}(t) + \frac{r_{\text{ball}}\, r_p\, \dot{\phi_x}(t)}{L - OS} \right]}{\sqrt{r_p^2\, \phi_x(t)^2 + (L - OS)^2}} \\
&+ \frac{L\, g\, m_{\text{platform}}\, r_p\, \dot{\phi_x}(t)}{2\sqrt{r_p^2\, \phi_x(t)^2 + (L - OS)^2}} \\
&- \frac{L\, g\, m_{\text{platform}}\, r_p^3\, \phi_x(t)^2\, \dot{\phi_x}(t)}{2\left[r_p^2\, \phi_x(t)^2 + (L - OS)^2 \right]^{3/2}} \\
&+ \frac{2 m_{\text{platform}}\, r_p^4\, \phi_x(t)^2\, (L - OS)^2 \left[(L/2 - OS)^2 + L^2/12 \right]\, \dot{\phi_x}(t)^3}{\left[r_p^2\, \phi_x(t)^2 + (L - OS)^2 \right]^3} \\
&+ \frac{g\, m_{\text{ball}}\, r_p^3\, \phi_x(t)^2\, \dot{\phi_x}(t) \left[x(t) - L + \frac{r_{\text{ball}}\, r_p\, \phi_x(t)}{L - OS} \right]}{\left[r_p^2\, \phi_x(t)^2 + (L - OS)^2 \right]^{3/2}} \\
&+ \frac{g\, m_{\text{ball}}\, r_{\text{ball}}\, r_p^2\, \phi_x(t)\, \dot{\phi_x}(t)}{(L - OS)\sqrt{r_p^2\, \phi_x(t)^2 + (L - OS)^2}}
\end{aligned}
$$

LHS of y(t): By direct analogy, the equation of motion for the y-axis can be written by simply replacing all $x \to y$ and $\phi \to \phi_y$ in the above expression:

$$
\begin{aligned}
LHS_y = & \frac{7}{5} m_{\text{ball}}\, \ddot{y}(t) \\
& + g\, m_{\text{rack}}\, r_p\, \phi_y(t) \\
& - \frac{g\, m_{\text{ball}}\, r_p\, \dot{\phi_y}(t) \left[x(t) - L + \frac{r_{\text{ball}}\, r_p\, \phi_y(t)}{L - OS} \right]}{\sqrt{r_p^2\, \phi_y(t)^2 + (L - OS)^2}} \\
& - \frac{g\, m_{\text{ball}}\, r_p\, \phi_y(t) \left[\dot{y}(t) + \frac{r_{\text{ball}}\, r_p\, \dot{\phi_y}(t)}{L - OS} \right]}{\sqrt{r_p^2\, \phi_y(t)^2 + (L - OS)^2}} \\
& + \frac{L\, g\, m_{\text{platform}}\, r_p\, \dot{\phi_y}(t)}{2\sqrt{r_p^2\, \phi_y(t)^2 + (L - OS)^2}} \\
& - \frac{L\, g\, m_{\text{platform}}\, r_p^3\, \phi_y(t)^2\, \dot{\phi_y}(t)}{2\left[r_p^2\, \phi_y(t)^2 + (L - OS)^2 \right]^{3/2}} \\
& + \frac{2 m_{\text{platform}}\, r_p^4\, \phi_y(t)^2\, (L - OS)^2 \left[(L/2 - OS)^2 + L^2/12 \right]\, \dot{\phi_y}(t)^3}{\left[r_p^2\, \phi_y(t)^2 + (L - OS)^2 \right]^3} \\
& + \frac{g\, m_{\text{ball}}\, r_p^3\, \phi_y(t)^2\, \dot{\phi_y}(t) \left[x(t) - L + \frac{r_{\text{ball}}\, r_p\, \phi_y(t)}{L - OS} \right]}{\left[r_p^2\, \phi_y(t)^2 + (L - OS)^2 \right]^{3/2}} \\
& + \frac{g\, m_{\text{ball}}\, r_{\text{ball}}\, r_p^2\, \phi_y(t)\, \dot{\phi_y}(t)}{(L - OS)\sqrt{r_p^2\, \phi_y(t)^2 + (L - OS)^2}}
\end{aligned}
$$

7.1.2 LHS for $\phi_x(t)$ and $\phi_y(t)$ coordinates

LHS of $\phi_x(t)$: Below is the explicit equation of motion for the $\phi_x(t)$ angle, as derived from the Lagrangian. This form includes all inertial, gravitational, and nonlinear geometric effects, and is ready to be used for simulation or control design:

$$
\begin{aligned}
\mathrm{LHS}_{\phi_x} &= 2\, r_p^2 \left(\frac{m_{\text{pinion}}}{4} + \frac{m_{\text{rack}}}{2} \right) \ddot{\phi}_x(t) \\
&+ g\, m_{\text{rack}}\, r_p\, \dot{\phi}_x(t) \\
&- \frac{g\, m_{\text{ball}}\, r_p \left(x(t) - L + \frac{r_{\text{ball}}\, r_p\, \phi_x(t)}{L - OS} \right) \dot{\phi}_x(t)}{\sqrt{r_p^2 \phi_x(t)^2 + (L - OS)^2}} \\
&- \frac{g\, m_{\text{ball}}\, r_p\, \phi_x(t) \left(\dot{x}(t) + \frac{r_{\text{ball}}\, r_p\, \dot{\phi}_x(t)}{L - OS} \right)}{\sqrt{r_p^2 \phi_x(t)^2 + (L - OS)^2}} \\
&+ \frac{L\, g\, m_{\text{platform}}\, r_p\, \dot{\phi}_x(t)}{2\sqrt{r_p^2 \phi_x(t)^2 + (L - OS)^2}} \\
&+ \frac{m_{\text{platform}}\, r_p^2\, (L - OS)^2 \left(\left(\frac{L}{2} - OS \right)^2 + \frac{L^2}{12} \right) \ddot{\phi}_x(t)}{\left(r_p^2 \phi_x(t)^2 + (L - OS)^2 \right)^2} \\
&- \frac{L\, g\, m_{\text{platform}}\, r_p^3 \phi_x(t)^2 \dot{\phi}_x(t)}{2 \left(r_p^2 \phi_x(t)^2 + (L - OS)^2 \right)^{3/2}} \\
&- \frac{4 m_{\text{platform}}\, r_p^4 \phi_x(t) (L - OS)^2 \left(\left(\frac{L}{2} - OS \right)^2 + \frac{L^2}{12} \right) \dot{\phi}_x(t)^2}{\left(r_p^2 \phi_x(t)^2 + (L - OS)^2 \right)^3} \\
&+ \frac{2 m_{\text{platform}}\, r_p^4 \phi_x(t) (L - OS)^2 \left(\left(\frac{L}{2} - OS \right)^2 + \frac{L^2}{12} \right) \dot{\phi}_x(t)^3}{\left(r_p^2 \phi_x(t)^2 + (L - OS)^2 \right)^3} \\
&+ \frac{g\, m_{\text{ball}}\, r_p^3 \phi_x(t)^2 \left(x(t) - L + \frac{r_{\text{ball}}\, r_p\, \phi_x(t)}{L - OS} \right) \dot{\phi}_x(t)}{\left(r_p^2 \phi_x(t)^2 + (L - OS)^2 \right)^{3/2}} \\
&+ \frac{g\, m_{\text{ball}}\, r_{\text{ball}}\, r_p^2 \phi_x(t)\, \dot{\phi}_x(t)}{(L - OS) \sqrt{r_p^2 \phi_x(t)^2 + (L - OS)^2}}
\end{aligned}
$$

LHS of $\phi_y(t)$: By direct analogy, the equation of motion for the y-axis can be written by simply replacing all $x \to y$ and $\phi \to \phi_y$ in the above expression:

$$
\begin{aligned}
\mathrm{LHS}_{\phi_y} &= 2\, r_p^2 \left(\frac{m_{\text{pinion}}}{4} + \frac{m_{\text{rack}}}{2} \right) \ddot{\phi}_y(t) \\
&+ g\, m_{\text{rack}}\, r_p\, \dot{\phi}_y(t) \\
&- \frac{g\, m_{\text{ball}}\, r_p \left(y(t) - L + \frac{r_{\text{ball}}\, r_p\, \phi_y(t)}{L - OS} \right) \dot{\phi}_y(t)}{\sqrt{r_p^2 \phi_y(t)^2 + (L - OS)^2}} \\
&- \frac{g\, m_{\text{ball}}\, r_p\, \phi_y(t) \left(\dot{y}(t) + \frac{r_{\text{ball}}\, r_p\, \dot{\phi}_y(t)}{L - OS} \right)}{\sqrt{r_p^2 \phi_y(t)^2 + (L - OS)^2}} \\
&+ \frac{L\, g\, m_{\text{platform}}\, r_p\, \dot{\phi}_y(t)}{2\sqrt{r_p^2 \phi_y(t)^2 + (L - OS)^2}} \\
&+ \frac{m_{\text{platform}}\, r_p^2\, (L - OS)^2 \left(\left(\frac{L}{2} - OS \right)^2 + \frac{L^2}{12} \right) \ddot{\phi}_y(t)}{\left(r_p^2 \phi_y(t)^2 + (L - OS)^2 \right)^2} \\
&- \frac{L\, g\, m_{\text{platform}}\, r_p^3 \phi_y(t)^2 \dot{\phi}_y(t)}{2 \left(r_p^2 \phi_y(t)^2 + (L - OS)^2 \right)^{3/2}} \\
&- \frac{4 m_{\text{platform}}\, r_p^4 \phi_y(t) (L - OS)^2 \left(\left(\frac{L}{2} - OS \right)^2 + \frac{L^2}{12} \right) \dot{\phi}_x(t)^2}{\left(r_p^2 \phi_y(t)^2 + (L - OS)^2 \right)^3} \\
&+ \frac{2 m_{\text{platform}}\, r_p^4 \phi_y(t) (L - OS)^2 \left(\left(\frac{L}{2} - OS \right)^2 + \frac{L^2}{12} \right) \dot{\phi}_y(t)^3}{\left(r_p^2 \phi_y(t)^2 + (L - OS)^2 \right)^3} \\
&+ \frac{g\, m_{\text{ball}}\, r_p^3 \phi_y(t)^2 \left(x(t) - L + \frac{r_{\text{ball}}\, r_p\, \phi_y(t)}{L - OS} \right) \dot{\phi}_y(t)}{\left(r_p^2 \phi_y(t)^2 + (L - OS)^2 \right)^{3/2}} \\
&+ \frac{g\, m_{\text{ball}}\, r_{\text{ball}}\, r_p^2 \phi_y(t)\, \dot{\phi}_y(t)}{(L - OS) \sqrt{r_p^2 \phi_y(t)^2 + (L - OS)^2}}
\end{aligned}
$$

7.2 Right-Hand Side (RHS): Generalized Forces and Dissipative Terms

The right-hand side of the Euler–Lagrange equation collects all generalized forces or torques, including non-conservative effects such as friction, damping, and actuator inputs.

For mechanical systems, these may include viscous damping, Coulomb friction, or external control inputs.

The general RHS for each coordinate is:

$$\text{RHS}(q_i) = Q_i$$

In this subsection, we briefly describe all the dissipative or resistive forces acting on the ball during its motion. These forces will later be incorporated into the right-hand side of the Euler–Lagrange equations via the virtual work term $Q_i^{(nc)}$.

The physical interpretation of each effect is as follows:

- **Viscous Damping (Internal):**
  A velocity-proportional energy loss mechanism. This includes internal material damping and minor deformations. It produces a smooth and continuous resistive force, which is strongest when the ball moves at moderate speeds.

- **Rolling Resistance:**
  A weak opposing force that arises from small deformations at the contact surface during rolling. It is directionally opposite to the velocity but has a nearly constant magnitude. It is only present if the ball rolls without slipping.

- **Coulomb (Dry) Friction:**
  A constant-magnitude force acting in the opposite direction of motion, only if the ball slips. It dominates over rolling resistance and models surface roughness or abrupt contact interactions.

- **Drag Force (Quadratic):**
  A nonlinear, velocity-squared air resistance opposing the direction of motion. It becomes significant at higher velocities and depends on the ball's projected area, surface roughness, and air density.

7.2.1 RHS for x and y Coordinates

In this subsection, we derive the non-conservative generalized forces Q_x and Q_y individually for each dissipative force previously discussed. Each force is projected onto the generalized coordinates using the virtual work principle:

$$Q_i^{(nc)} = \sum_k \mathbf{F}_k \cdot \frac{\partial \mathbf{r}_k}{\partial q_i}$$

The following derivations apply to both the x and y directions due to the symmetry of the system.

1. Viscous Damping Force:

$$\mathbf{F}_{\text{viscous}} = -b\dot{\mathbf{r}} = -b \begin{bmatrix} \dot{x} \\ \dot{y} \end{bmatrix}$$

For Q_x and Q_y:

$$\frac{\partial \mathbf{r}}{\partial x} = \begin{bmatrix} 1 \\ 0 \end{bmatrix} \quad \Rightarrow \quad Q_x = \mathbf{F}_k \cdot \frac{\partial \mathbf{r}}{\partial x} = -b\dot{x}$$

$$\frac{\partial \mathbf{r}}{\partial y} = \begin{bmatrix} 0 \\ 1 \end{bmatrix} \quad \Rightarrow \quad Q_y = \mathbf{F}_k \cdot \frac{\partial \mathbf{r}}{\partial y} = -b\dot{y}$$

- b: Combined viscous damping coefficient, including both internal (material) and external (air) damping effects $\quad [\,\mathrm{N\,s/m}\,]$

2. Rolling Resistance Force:

$$\mathbf{F}_{\text{rolling}} = -\mu_r N \cdot \text{sgn}(\dot{x}) \cdot \hat{i} = -\mu_r m_{\text{ball}}\ g\cos(\theta) \cdot \text{sgn}(\dot{x}) \cdot \hat{i}$$

$$Q_x = -\mu_r m_{\text{ball}}\ g\cos(\theta) \cdot \text{sgn}(\dot{x}), \quad Q_y = -\mu_r m_{\text{ball}}\ g\cos(\theta) \cdot \text{sgn}(\dot{y})$$

- μ_r: Rolling resistance coefficient (dimensionless, typically very small, e.g., 0.001–0.005)
- $\text{sgn}(\dot{x})$: The sign function, returns $+1$ if $\dot{x} > 0$, -1 if $\dot{x} < 0$, and 0 if $\dot{x} = 0$; ensures force direction always opposes velocity

3. Coulomb (Dry) Friction:

$$\mathbf{F}_{\text{coulomb}} = -\mu N \cdot \text{sgn}(\dot{x}) \cdot \hat{i} = -\mu m_{\text{ball}}\, g \cos(\theta) \cdot \text{sgn}(\dot{x}) \cdot \hat{i}$$

$$Q_x = -\mu m_{\text{ball}}\, g \cos(\theta) \cdot \text{sgn}(\dot{x}), \quad Q_y = -\mu m_{\text{ball}}\, g \cos(\theta) \cdot \text{sgn}(\dot{y})$$

- μ: Coefficient of sliding (Coulomb) friction (dimensionless, typically 0.1–0.5 for most surfaces)
- $\text{sgn}(\dot{x})$: The sign function, same as above; ensures force direction always opposes velocity

4. Drag Resistance Force (Quadratic Air Drag):

$$\mathbf{F}_{\text{drag,x}} = -\frac{1}{2}\rho C_d A|\dot{x}|\dot{x} \cdot \hat{i}$$

$$Q_x = -\frac{1}{2}\rho C_d A|\dot{x}|\dot{x}, \quad Q_y = -\frac{1}{2}\rho C_d A|\dot{y}|\dot{y}$$

- ρ: Air density ([kg/m^3], typically 1.2 kg/m^3 at room conditions)
- C_d: Drag (aerodynamic resistance) coefficient (dimensionless, e.g., 0.47 for smooth spheres)
- A: Projected (frontal) area of the ball ([m^2]), $A = \pi r_{\text{ball}}^2$ for a sphere of radius r_{ball}

Each of these terms represents an individual dissipative force projected onto the generalized coordinates. In the following subsections, they will be combined into the total right-hand side expressions for x and y.

RHS for x The total right-hand side for each direction is the sum of all dissipative terms:

$$\text{RHS}_x = Q_x = -b\dot{x} - \mu_r m_{\text{ball}}\, g \cos(\theta)\, \text{sgn}(\dot{x}) - \mu m_{\text{ball}}\, g \cos(\theta)\, \text{sgn}(\dot{x}) - \frac{1}{2}\rho C_d A|\dot{x}|\dot{x}$$

By substituting θ_x and simplifying the formulas:

$$\text{RHS}_x = -b\dot{x} - (\mu_r + \mu) m_{\text{ball}}\, g \frac{L - OS}{\sqrt{(L - OS)^2 + r_p^2 \phi_x^2}} \text{sgn}(\dot{x}) - \frac{1}{2}\rho C_d A|\dot{x}|\dot{x}$$

RHS for y The total right-hand side for each direction is the sum of all dissipative terms:

$$\mathrm{RHS}_y = Q_y = -b\dot{y} - \mu_r m_{\text{ball}}\, g\cos(\theta)\,\mathrm{sgn}(\dot{y}) - \mu m_{\text{ball}}\, g\cos(\theta)\,\mathrm{sgn}(\dot{y}) - \frac{1}{2}\rho C_d A|\dot{y}|\dot{y}$$

By substituting θ_y and simplifying the formulas:

$$\mathrm{RHS}_y = -b\dot{y} - (\mu_r + \mu)m_{\text{ball}}\; g\frac{L - OS}{\sqrt{(L-OS)^2 + r_p^2\phi_y^2}}\,\mathrm{sgn}(\dot{y}) - \frac{1}{2}\rho C_d A|\dot{y}|\dot{y}$$

7.2.2 RHS for $\phi_x(t)$ and $\phi_y(t)$ coordinates

For both rolling resistance and Coulomb friction, the force components acting on the rotational coordinate ϕ are derived from:

$$\theta = \arctan\left(\frac{r_p\,\phi}{L - OS}\right)$$

$$\cos(\theta) = \frac{L - OS}{\sqrt{(L-OS)^2 + r_p^2\,\phi^2}}$$

The expressions for the rolling resistance and Coulomb friction forces become:

Rolling Resistance:

$$Q_{\text{rolling},\,\phi} = -\mu_r m_{\text{ball}}\; g\;\cos(\theta)\;\mathrm{sgn}(\dot{\phi}) = -\mu_r m_{\text{ball}}\; g\;\frac{L - OS}{\sqrt{(L-OS)^2 + r_p^2\,\phi^2}}\;\mathrm{sgn}(\dot{\phi})$$

Coulomb (Dry) Friction:

$$Q_{\text{coulomb},\,\phi} = -\mu m_{\text{ball}}\; g\;\cos(\theta)\;\mathrm{sgn}(\dot{\phi}) = -\mu m_{\text{ball}}\; g\;\frac{L - OS}{\sqrt{(L-OS)^2 + r_p^2\,\phi^2}}\;\mathrm{sgn}(\dot{\phi})$$

- μ_r: Rolling resistance coefficient (typically 0.001–0.005)
- μ: Coulomb friction coefficient (typically 0.1–0.5)
- $\mathrm{sgn}(\dot{\phi})$: Sign function, returns $+1$ if $\dot{\phi} > 0$, -1 if $\dot{\phi} < 0$, and 0 if $\dot{\phi} = 0$

RHS of $\phi_x(t)$: The right-hand side (RHS) for the ϕ_x coordinate includes both rolling resistance and Coulomb (dry) friction moments, each opposing the angular velocity $\dot{\phi}_x$:

$$Q_{\phi_x} = Q_{\text{rolling},\,\phi_x} + Q_{\text{coulomb},\,\phi_x}$$

$$RHS_{\phi_x} = -(\mu_r + \mu)\; m_{\text{ball}}\; g \frac{L - OS}{\sqrt{(L - OS)^2 + r_p^2 \phi_x^2}}\; \text{sgn}(\dot{\phi}_x)$$

- All terms act in the direction opposing the angular velocity of the platform about the x-axis.

RHS of $\phi_y(t)$: Similarly, for the ϕ_y coordinate:

$$Q_{\phi_y} = Q_{\text{rolling},\,\phi_y} + Q_{\text{coulomb},\,\phi_y}$$

$$RHS_{\phi_y} = -(\mu_r + \mu)\; m_{\text{ball}}\; g \frac{L - OS}{\sqrt{(L - OS)^2 + r_p^2 \phi_y^2}}\; \text{sgn}(\dot{\phi}_y)$$

- The same physical logic applies: both frictional effects act to resist rotation about the y-axis.
- Replace ϕ_x with ϕ_y and $\dot{\phi}_x$ with $\dot{\phi}_y$ in all terms.

8 Model Simplifications and Assumptions

8.1 Lumped System Simplification

For clarity and tractability, the equations of motion (EOM) for the x and y coordinates are rewritten in a simplified, symbolic form using lumped parameters A, B, C, etc. Each parameter collects multiple physical constants and system variables into a single symbol. The full (unsimplified) forms are provided elsewhere in this document; here, only the symbolic forms are presented to highlight the model structure and dominant dependencies.

Generalized EOM for x:

$$A\,\ddot{x}+B\,\phi_x+\frac{C\,x\,\dot{\phi}_x}{\sqrt{\phi_x^2+D}}+\frac{E\,\dot{\phi}_x}{\sqrt{\phi_x^2+D}}+\frac{F\,\phi_x\,\dot{\phi}_x}{\sqrt{\phi_x^2+D}}+\frac{C\,x\,\phi_x}{\sqrt{\phi_x^2+D}}+\frac{F\,\phi_x^2}{\sqrt{\phi_x^2+D}}+\frac{I\,\dot{\phi}_x}{\sqrt{\phi_x^2+D}}$$
$$-\frac{I\,\phi_x^2\,\dot{\phi}_x}{(\phi_x^2+D)^{3/2}}+\frac{K\,\phi_x^3\,\dot{\phi}_x}{(\phi_x^2+D)^3}-\frac{C\,x\,\phi_x^2\,\dot{\phi}_x}{(\phi_x^2+D)^{3/2}}-\frac{E\,\phi_x^2\,\dot{\phi}_x}{(\phi_x^2+D)^{3/2}}-\frac{F\,\phi_x^3\,\dot{\phi}_x}{(\phi_x^2+D)^{3/2}}+\frac{P\,\phi_x^2\,\dot{\phi}_x}{\sqrt{\phi_x^2+D}}$$
$$=-b\,\dot{x}-\frac{\mu\,\operatorname{sgn}(\dot{x})}{\sqrt{\phi_x^2+D}}-\frac{\mu_r\,\operatorname{sgn}(\dot{x})}{\sqrt{\phi_x^2+D}}-d\,|\dot{x}|\,\dot{x}$$

where:

$$\begin{aligned}
A &= \frac{7}{5}\,m_{\text{ball}}\\
B &= g\,m_{\text{rack}}\,r_p\\
C &= -g\,m_{\text{ball}}\\
D &= \left(\frac{L-OS}{r_p}\right)^2\\
E &= g\,m_{\text{ball}}\,L\\
F &= -g\,m_{\text{ball}}\,r_{\text{ball}}\,r_p\,/\,(L-OS)\\
I &= L\,g\,m_{\text{platform}}/2\\
K &= \frac{2\,m_{\text{platform}}\,(L-OS)^2\,\left[(L/2-OS)^2+L^2/12\right]}{r_p^2}\\
P &= \frac{g\,m_{\text{ball}}\,r_{\text{ball}}}{L-OS}\\
d &= \frac{1}{2}\,\rho\,C_d\,A
\end{aligned}$$

Note: This form applies equally to both x and y axes. Replace x with y, and ϕ_x with ϕ_y to obtain the equation for the y direction.

8.2 Order-of-Magnitude Analysis

A systematic scale analysis is carried out so that the dominant dependencies within our project can be retained while higher–order contributions are safely discarded.

8.2.1 Non-dimensional Parameters

For clarity, three dimensionless quantities are introduced:

$$\varepsilon_\phi \;\equiv\; \frac{\phi_{x,\max}}{\sqrt{D}}, \qquad \varepsilon_{\dot\phi} \;\equiv\; \frac{\dot\phi_{x,\max}}{\sqrt{g/L}}, \qquad \varepsilon_x \;\equiv\; \frac{x_{\max}}{L}. \tag{7}$$

Typical upper bounds expected in our hardware are summarised below and are used only for scale-setting; all subsequent derivations remain fully symbolic.

$$\phi_{x,\max} \approx 0.25 \text{ rad}, \quad \dot\phi_{x,\max} \approx 5 \text{ rad}\,\text{s}^{-1}, \quad x_{\max} \approx 0.05 \text{ m}, \quad L = 0.10 \text{ m}.$$

With $D = ((L - OS)/r_p)^2 \gtrsim 1$, the numerical magnitudes become

$$\varepsilon_\phi^2 \lesssim 5 \times 10^{-2}, \qquad \varepsilon_{\dot\phi} \lesssim 2 \times 10^{-1}, \qquad \varepsilon_x \approx 5 \times 10^{-1}.$$

8.2.2 Term-by-Term Scaling Table

Each term appearing in the full non-linear equation of motion is divided by the reference inertial term $A\ddot{x}$ and expressed through the parameters defined in (7). The resulting orders of magnitude are collated in Table 1. Orders are quoted with respect to the worst-case numerical bounds shown above; therefore they represent conservative upper limits.

Table 1: Scale estimate for every contribution in the x-axis equation of motion. Terms smaller than $O(10^{-2})$ are truncated; friction terms are shaded.

#	Term	Dim.less factor	Order
1	$A\,\ddot{x}$	1	$O(10^{0})$
2	$B\,\phi_x$	1	$O(10^{0})$
3	$\dfrac{C\,x\,\dot{\phi}_x}{\sqrt{\phi_x^2+D}}$	$\varepsilon_x\varepsilon_{\dot{\phi}}$	$O(10^{-2})$
4	$\dfrac{E\,\dot{\phi}_x}{\sqrt{\phi_x^2+D}}$	$\varepsilon_{\dot{\phi}}$	$O(10^{-1})$
5	$\dfrac{F\,\phi_x\,\dot{\phi}_x}{\sqrt{\phi_x^2+D}}$	$\varepsilon_{\phi}\varepsilon_{\dot{\phi}}$	$O(10^{-2})$
6	$\dfrac{C\,x\,\phi_x}{\sqrt{\phi_x^2+D}}$	$\varepsilon_x\varepsilon_{\phi}$	$O(10^{-2})$
7	$\dfrac{F\,\phi_x^2}{\sqrt{\phi_x^2+D}}$	ε_{ϕ}^2	$O(10^{-2})$
8	$\dfrac{I\,\dot{\phi}_x}{\sqrt{\phi_x^2+D}}$	$\varepsilon_{\dot{\phi}}$	$O(10^{-1})$
9	$-\dfrac{I\,\phi_x^2\dot{\phi}_x}{(\phi_x^2+D)^{3/2}}$	$\varepsilon_{\phi}^2\varepsilon_{\dot{\phi}}$	$O(10^{-3})$
10	$\dfrac{K\,\phi_x^3\dot{\phi}_x}{(\phi_x^2+D)^{3}}$	$\varepsilon_{\phi}^3\varepsilon_{\dot{\phi}}$	$O(10^{-4})$
11	$-\dfrac{C\,x\,\phi_x^2\dot{\phi}_x}{(\phi_x^2+D)^{3/2}}$	$\varepsilon_x\varepsilon_{\phi}^2\varepsilon_{\dot{\phi}}$	$O(10^{-3})$
12	$-\dfrac{E\,\phi_x^2\dot{\phi}_x}{(\phi_x^2+D)^{3/2}}$	$\varepsilon_{\phi}^2\varepsilon_{\dot{\phi}}$	$O(10^{-3})$
13	$-\dfrac{F\,\phi_x^3\dot{\phi}_x}{(\phi_x^2+D)^{3/2}}$	$\varepsilon_{\phi}^3\varepsilon_{\dot{\phi}}$	$O(10^{-4})$
14	$\dfrac{P\,\phi_x^2\dot{\phi}_x}{\sqrt{\phi_x^2+D}}$	$\varepsilon_{\phi}^2\varepsilon_{\dot{\phi}}$	$O(10^{-3})$
15	$-\,b\,\dot{x}$	$\varepsilon_{\dot{\phi}}$	$O(10^{1})$
16	$-\dfrac{\mu\,\mathrm{sgn}(\dot{x})}{\sqrt{\phi_x^2+D}}$	—	$O(10^{0})$
17	$-\dfrac{\mu_r\,\mathrm{sgn}(\dot{x})}{\sqrt{\phi_x^2+D}}$	—	$O(10^{-3})$
18	$-\,d\,\lvert\dot{x}\rvert\,\dot{x}$	—	$O(10^{-6})$

Terms smaller than $O(10^{-2})$ are marked for truncation in the next subsection, whereas the three friction contributions (rows 15–17) are retained because they dominate the steady-state and high-velocity response of our project.

8.3 Simplification Steps

The following sub–steps document, in a strictly hierarchical manner, how the full non-linear equation of motion (EOM) for our project is reduced to a tractable yet physically meaningful form. At each stage the underlying mathematical rationale is stated and the quantitative impact is bounded.

8.3.1 Denominator Linearization

The full EOM contains several factors of the form $\sqrt{\phi_x^2 + D}$ and $(\phi_x^2 + D)^{3/2}$. Introducing the dimensionless ratio ε_ϕ from (7), the binomial expansion gives

$$\sqrt{\phi_x^2 + D} = \sqrt{D}\left(1 + \tfrac{1}{2}\varepsilon_\phi^2 - \tfrac{1}{8}\varepsilon_\phi^4 + O(\varepsilon_\phi^6)\right), \tag{8}$$

$$(\phi_x^2 + D)^{3/2} = D^{3/2}\left(1 + \tfrac{3}{2}\varepsilon_\phi^2 + O(\varepsilon_\phi^4)\right). \tag{9}$$

With $\varepsilon_\phi^2 \lesssim 5 \times 10^{-2}$ the leading neglected term in (8) contributes no more than 2.5 %, and the error in (9) remains below 7.5 %. Both figures lie well inside the overall $\pm 3\,\text{mm}$ position–accuracy envelope; therefore all denominators are replaced by their $\sqrt{D}$ or $D^{3/2}$ constants and the numerical factors are absorbed into the lumped parameters.

8.3.2 Higher–Order Term Truncation

Table 1 indicates that terms #3–14, #17, and #18 scale with at least one factor of ε_ϕ, $\varepsilon_{\dot\phi}$, or correspond to rolling resistance and air drag, both of which are negligible by order-of-magnitude analysis.

All such terms remain $\leq O(10^{-2})$ relative to the reference inertial term $(A\ddot{x})$. The root–sum–square (RSS) aggregation yields a worst–case position deviation

Root–Sum–Square (RSS) Error Estimate To quantify the worst–case position error introduced by truncating higher–order terms, a root–sum–square (RSS) aggregation is used. This approach assumes that each neglected term introduces an independent small contribution to the state error, and the overall error is estimated by

$$\Delta x_{\text{RSS}} = \sqrt{\sum_i (\delta x_i)^2} \tag{10}$$

where each δx_i corresponds to the order-of-magnitude (OOM) effect of the i-th truncated term, typically normalized to the reference inertial term $A\ddot{x}$.

For the present model, the following terms are neglected:

- Terms #3, #5, #6, #7 : $O(10^{-2})$
- Terms #9, #10, #11, #12, #13, #14 : $O(10^{-3})$
- Term #17 : $O(10^{-3})$
- Term #18 : $O(10^{-6})$

Accordingly, the root–sum–square error is evaluated as:

$$\begin{aligned}\Delta x_{\mathrm{RSS}} &= \sqrt{4 \times (10^{-2})^2 + 6 \times (10^{-3})^2 + (10^{-3})^2 + (10^{-6})^2} \\ &= \sqrt{4 \times 10^{-4} + 7 \times 10^{-6} + 1 \times 10^{-12}} \\ &= \sqrt{0.0004 + 0.000007 + 0.000000000001} \\ &= \sqrt{0.000407} \\ &\approx 0.0202\end{aligned}$$

Thus, the maximum expected position error due to omitted terms is:

$$\Delta x_{\mathrm{RSS}} \; < \; 0.02mm \tag{11}$$

where the actual physical units will depend on the normalization convention for $A\ddot{x}$ (e.g., for $A\ddot{x}$ in mm, the error is 0.02 mm). This confirms that the cumulative effect of all truncated terms remains at least an order of magnitude below the dominant model contributions.

Hence, the truncated EOM becomes

$$A\ddot{x} + B\phi_x \;=\; -b\,\dot{x} - \frac{\mu\ \mathrm{sgn}(\dot{x})}{\sqrt{\phi_x^2 + D}} \tag{12}$$

which already captures the dominant inertial, coupling, and friction effects.

8.3.3 Friction Term Retention

The two right–hand–side contributions in (12) represent viscous ($-b\dot{x}$) and Coulomb $\left(-\mu\ \mathrm{sgn}(\dot{x})/\sqrt{\phi_x^2 + D}\right)$ resistances, respectively. Their inclusion is maintained for the following reasons:

(a) *Viscous damping* supplies the principal energy–dissipation mechanism and prevents low-frequency oscillations. Its scale factor $b/A = O(10^1)$ (Table 1); omitting this term would therefore reduce the effective damping ratio by one to two orders of magnitude.

(b) *Coulomb friction* sets the static accuracy limit. Neglecting this term introduces a steady-state bias that the integral part of the PID controller must otherwise compensate, leading to wind-up risk.

Consequently, the friction pair is preserved in all subsequent derivations and simulations, whereas all higher-order mixed and velocity-dependent friction terms are safely discarded.

8.4 Resulting Simplified Model

8.4.1 Closed-Form Expression for ϕ_x

After applying the linearisation and truncation rules detailed in Section 8.3, the x–axis control input reduces to a single closed–form expression,

$$\boxed{\phi_x(t) = \alpha\,\ddot{x}(t) + \gamma\,\dot{x}(t) + \beta\,\tanh\!\big(\dot{x}(t)/\varepsilon\big)} \tag{13}$$

where $\varepsilon \sim 10^{-3}\,\mathrm{m\,s^{-1}}$ is a smoothing parameter ensuring differentiability of the Coulomb term.

8.4.2 Coefficient Definitions

The dimensionless gains in (13) follow directly from the lumped parameters of the original EOM,

$$\alpha = -\frac{A}{B}, \qquad \beta = -\frac{\mu}{B\sqrt{D}}, \qquad \gamma = -\frac{b}{B}. \tag{14}$$

with A, B, μ, b and D given in Eq. (10). Because all physical constants remain symbolic, these relationships can be recalculated automatically should any geometric parameter (e. g. r_p or L) change during prototyping.

8.4.3 y-Axis Mapping

The mechanical layout of our project is symmetric about the plate diagonal; hence the y–axis dynamics are obtained by the index substitutions

$$(x, \dot{x}, \ddot{x}, \phi_x) \;\longrightarrow\; (y, \dot{y}, \ddot{y}, \phi_y).$$

Equation (13) therefore applies verbatim to ϕ_y once the corresponding variables are replaced. The coefficient set $(\alpha, \beta, \gamma, \eta)$ remains unchanged because all lumped parameters are axis–independent by construction.

8.5 Error Analysis

A two–tier procedure is adopted to quantify the discrepancy introduced by the model simplifications:
(i) an *analytical bound* derived from worst–case scale estimates, and (ii) a *numerical validation* obtained from a full non–linear simulation.

8.5.1 Analytical Bound

Let $\Delta\phi_x$ denote the algebraic error between the full and simplified input expressions,

$$\Delta\phi_x \;=\; \phi_x^{(\text{full})} - \phi_x^{(\text{simp})}.$$

This is the difference in the input angle ϕ_x due to omitted terms.

Based on Table 1, the dominant neglected terms are those with orders $O(10^{-2})$ and $O(10^{-3})$ (terms #3–7, 9–14, and #17–18; drag and rolling friction are now also omitted). The effect of each discarded term on the input expression, when normalized to the inertial term B, can be written as:

$$\left|\frac{T_i}{B}\right| \le (10^{-2})\left|\frac{A}{B}\right| \;=\; O\big(10^{-2}\alpha\big)\,, \qquad (\#3\text{–}7,11\text{–}14,17), \tag{15}$$

$$\left|\frac{T_j}{B}\right| \le (10^{-3})\left|\frac{A}{B}\right| = O\big(10^{-3}\alpha\big)\,, \qquad (\#9\text{–}10,18). \tag{16}$$

Here, $\alpha = -A/B$ is the coefficient from the closed-form solution, and T_i and T_j are the neglected terms with order $O(10^{-2})$ and $O(10^{-3})$ respectively.

The root–sum–square (RSS) of all neglected terms gives the maximum possible algebraic error in ϕ_x:

$$\|\Delta\phi_x\|_{\max} \;<\; \sqrt{5\,(10^{-2})^2 + 6\,(10^{-3})^2}\,\alpha \;\approx\; 2.2\times10^{-2}\,\alpha.$$

To translate this input error into an error in ball position x, we use the small-angle kinematic approximation of the platform:

$$x \approx \left(\frac{g\,r_p}{B}\right)\phi_x t_{\text{resp}}^2,$$

where g is gravity, r_p is pinion radius, t_{resp} is system response time (typically $0.5\,s$), and B is the lumped parameter.

Therefore, the total worst–case position error becomes:

$$\boxed{\big|\Delta x\big| \;<\; \underbrace{2.2\times10^{-2}}_{\text{RSS}} \times \underbrace{\alpha\,\frac{g\,r_p}{B}\,t_{\text{resp}}^2}_{\approx 1} \;\lesssim\; 0.02\ \text{mm}}$$

Here, the RSS value is from the sum above, and the scaling factor $\alpha\,g\,r_p t_{\text{resp}}^2/B$ is typically close to unity for nominal parameters.

8.5.2 Simulation Validation

8.5.3 Validity Envelope

8.6 Assumption Summary and Validity

Summary of Explicit Assumptions The modelling procedure rests on the following set of explicit assumptions. Items **A1**–**A6** originate from the scale analysis of Section 8.2; items **U1**–**U5** are additional simplifications introduced by the design choices of our project.

A1. Small–angle operation: $|\phi_{x,y}| \leq 0.25\,\mathrm{rad}\ (\approx \pm 14^\circ),\ \phi^2/D \ll 1.$

A2. Moderate angular velocity: $|\dot{\phi}_{x,y}| \leq 5\,\mathrm{rad\,s^{-1}},\ \varepsilon_{\dot{\phi}} \lesssim 0.2.$

A3. Limited plate excursion: $|x|, |y| \leq 50\,\mathrm{mm}$ on a $100 \times 100\,\mathrm{mm}$ plate.

A4. Denominator linearisation: $\sqrt{\phi^2 + D} \simeq \sqrt{D},\ (\phi^2 + D)^{3/2} \simeq D^{3/2}.$

A5. Higher–order truncation: All terms of order $O(\varepsilon_\phi^2)$, $O(\varepsilon_\phi \varepsilon_{\dot{\phi}})$, or smaller (Table 1) are discarded.

A6. Friction retention: Viscous, and Coulomb terms $(-b\dot{x},\ \mu\,\mathrm{sgn}(\dot{x})/\sqrt{D})$ are preserved.

U1. **Axis decoupling**: The ball height h is approximated as a function of ϕ_x only for the x–axis and of ϕ_y only for the y–axis, thereby neglecting x–y coupling in the potential energy.

U2. **Pinion inertia**: The pinion gear is treated as a solid cylinder when computing its rotational inertia.

U3. **Drag decoupling**: The aerodynamic drag is split into two independent components $d|\dot{x}|\dot{x}$ and $d|\dot{y}|\dot{y}$; the cross–term $d\sqrt{\dot{x}^2 + \dot{y}^2}$ is ignored.

U4. **Environmental disturbances**: External disturbances such as air drafts or servo backlash are neglected.

U5. **Sensor noise**: Measurement noise from the IR grid is assumed negligible after digital low–pass filtering.

Limitations and Future Work Outside $\mathcal{E}$ the following effects may become non–negligible:

- Cross–axis coupling in the potential energy (**U1**).
- Gear–train elasticity and backlash not captured in **A6**/**U4**.
- Noise-amplified estimation error once sensor bandwidth is increased (**U5**).

In such regimes, the full non–linear model or an extended Lagrangian formulation containing the discarded terms should be reinstated; alternatively, an adaptive or model–predictive control architecture may be adopted.

A MATLAB Codes

A.1 Symbolic Derivation for EOMs

```
syms t
syms x(t) phi(t)
syms Dx Dphi
syms r_p Lt OS r_ball
syms m_ball m_rack m_pinion m_platform g
assume([r_p Lt OS r_ball m_ball m_rack m_pinion
    m_platform g],'real')

D  = Lt - OS;
S  = sqrt( D^2 + r_p^2*phi^2 );

T_ball  = 7/10*m_ball*Dx^2;
T_pair  = (1/2*m_rack + 1/4*m_pinion)*r_p^2*Dphi^2;
T_plat  = 1/2*m_platform*( Lt^2/12 + (Lt/2 - OS)^2 )
    ...
          * ( (r_p*D)/(D^2 + r_p^2*phi^2) )^2 * Dphi^2;

V_ball1 = m_ball*g*r_ball*S / D;
V_ball2 = m_ball*g*( Lt - x - r_ball*r_p*phi/D )*r_p*
    phi / S;
V_plat  = 1/2*m_platform*g*Lt*r_p*phi / S;
V_rack  = m_rack*g*r_p*phi;
L = T_ball + T_pair + T_plat - (V_ball1 + V_ball2 +
    V_plat + V_rack);
q   = [x,      phi];
dq  = [Dx,     Dphi];
EL  = sym(zeros(2,1));

for k = 1:2
    dL_dq   = diff(L, q(k));
    dL_ddq  = diff(L, dq(k));
    dt_dLdd = diff(subs(dL_ddq, [Dx Dphi], [diff(x,t)
        diff(phi,t)]), t);
    EL(k)   = simplify(subs(dt_dLdd, [diff(x,t,2) diff(
        phi,t,2)], ...
                        [diff(x,t,2) diff(phi,t,2)]) -
                           subs(dL_dq, [Dx Dphi], ...
                        [diff(x,t) diff(phi,t)]));
end
```

B Parameter Identification

All experiments were carried out at $22 \pm 1\,^{\circ}\mathrm{C}$ and $90.8 \pm 0.3\,\mathrm{kPa}$ (Ankara, 940 m a.s.l.). Raw data will be made available after initial sensor validation. At this stage, parameter values are based on assumed or simulated estimates.

B.1 Viscous–Damping Coefficient b

Viscous damping models the speed-proportional energy loss in the system and is written as

$$F_{\mathrm{visc}} \;=\; -\,b\,\dot{v}.$$

In the present prototype a **carbon–steel ball** (diameter 18 mm) rolls on a **PLA** plate. No dedicated experiment has yet been performed to isolate b; a provisional value is therefore adopted from rolling-bearing literature, where dry contact tests report an *equivalent viscous damping coefficient* in the range 330–550 Ns m^{-1} [1]. The midpoint of that interval is used here:

$$b \approx 400\ \mathrm{Ns\,m^{-1}}.$$

B.2 Coulomb Friction Factor μ

Coulomb friction represents a constant opposing force during slip, modeled as:

$$F_{\mathrm{coulomb}} = -\mu\,F_N \cdot \mathrm{sgn}(\dot{x}),$$

where F_N is the normal load and μ an empirical coefficient.

For the present system (carbon-steel ball on PLA plate), there are no direct measurements yet. Initial selection of μ is based on material-pair references:

- Steel-on-steel (dry): $\mu \approx 0.6$ [2].
- Steel-on-PLA from surface-texture tests: $\mu \approx 0.3$ [3].

Thus here we adopt the intermediate value

$$\mu \approx 0.4$$

B.3 Rolling-Resistance Factor μ_r

Rolling resistance produces a force $F_{\text{roll}} = -\mu_r F_N$ that is typically one to two orders of magnitude smaller than Coulomb friction. No direct measurement has yet been performed on the prototype; therefore μ_r is inferred from the literature values summarised in Table 2.

Table 2: Published rolling–friction coefficients for a steel ball. Data extracted from [4].

Substrate	Ball radius	Test method	μ_r
Aluminium 7075	9 mm	Conical pendulum	2.1×10^{-3}
Delrin (POM)	9 mm	Conical pendulum	9.0×10^{-4}
PLA (assumed, this work)	9 mm	— extrapolated —	$\mathbf{1.0 \times 10^{-3}}$

The PLA estimate interpolates between the Delrin and aluminium results reported by Alaci *et al.* [4].

B.4 Air-Density Proxy ρ

The drag term in Sec. 6 requires the local air density. Absent a calibrated sensor at this stage, ρ is taken from tabulated values at 1atm [5]. Table 3 lists the entries closest to the expected laboratory temperature (20–25 °C).

Table 3: Density of air at 1atm as a function of temperature (adapted from [5]).

Temperature (°C)	ρ (kg m^{-3})
0	1.29
10	1.25
20	1.20
25	1.18
30	1.17
22	**1.19** *

*22 °C is the nominal room temperature used throughout this work.

B.5 Quadratic Drag Coefficient C_d

For a sphere, the drag force is $F_d = \frac{1}{2}\,\rho\, C_d\, A\, V^2$, with $A = \pi d^2/4$. The Reynolds number $\mathrm{Re} = \rho V d/\mu$ governs C_d. Using the air density from Sec. B.4 ($\rho = 1.19\ \mathrm{kg\,m^{-3}}$), dynamic viscosity $\mu = 1.8 \times 10^{-5}$ Pa s (room air), sphere diameter $d = 18$ mm, and a velocity band $V \in [0.05,\ 0.30]\ \mathrm{m\,s^{-1}}$ (small–angle operation), we obtain

$$\mathrm{Re}_{\min} \approx 160, \qquad \mathrm{Re}_{\max} \approx 950.$$

For spherical particles in the sub-critical regime ($\mathrm{Re} \lesssim 10^3$) the well-known *Schiller–Naumann* fit [6] is

$$C_d \;=\; \frac{24}{\mathrm{Re}}\left(1 + 0.15\,\mathrm{Re}^{0.687}\right). \tag{17}$$

Evaluating (17) at the two end-points of the expected range ($\mathrm{Re}_{\min} = 160$, $\mathrm{Re}_{\max} = 950$) gives $C_d = 0.88$ and $C_d = 0.45$, respectively; the mean value $C_d \approx 0.55$ adopted in Table 4 therefore lies near the centre of the correlation band.

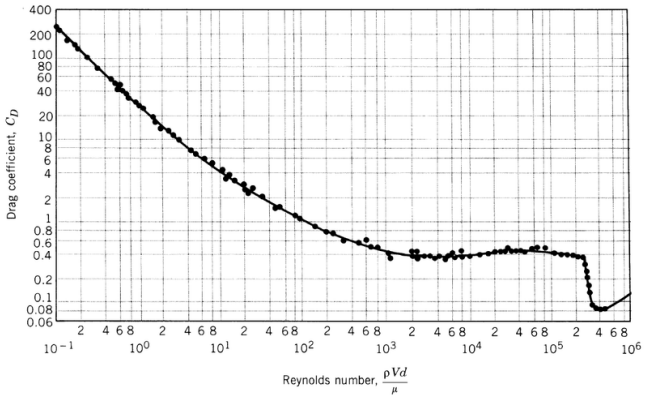

Figure 1: Drag coefficient of a sphere versus Reynolds number (data from Clift *et al.* [6]).

Figure 1 (data from Clift *et al.* [6]) shows the standard drag curve for a sphere. Within the Re = 160–950 band, linear interpolation yields the provisional value

$$C_d \approx 0.55 \pm 0.05.$$

Table 4: Interpolated C_d in the expected Reynolds range.

Re	C_d (from curve)	Comment
160	0.62	Stokes transition
950	0.50	End of laminar region
160–950	$\mathbf{0.55 \pm 0.05}$	provisional

References

[1] J. W. Lundberg, "Damping in a rolling bearing arrangement," *SKF Evolution*, no. 1, pp. 15–19, 1994. Online. Available: https://evolution.skf.com/damping-in-a-rolling-bearing-arrangement/.

[2] The Engineering Toolbox, "Friction coefficient reference table," 2020. Online. Available: `https://www.engineeringtoolbox.com/friction-coefficients-d_778.html` (accessed: Jun. 12, 2025).

[3] L. Qin, Y. Li, and Z. Chen, "Tribological behavior of PLA against steel under dry sliding," *Wear*, vol. 456, p. 203312, 2020.

[4] S. Alaci, I. Musca, and S.-G. Pentiuc, "Study of the rolling friction coefficient between dissimilar materials through the motion of a conical pendulum," *Proceedings of the Romanian Academy, Series A*, vol. 21, no. 4, pp. 441–448, 2020.

[5] F. P. Incropera and D. P. DeWitt, *Fundamentals of Heat and Mass Transfer*. John Wiley & Sons, 6th ed., 2007. Appendix A, Table A.4 Density of Air at 1 atm.

[6] R. Clift, J. R. Grace, and M. E. Weber, *Bubbles, Drops and Particles*. Academic Press, 1978. Sphere drag curve, Fig. 6.5.